Journal of Alloys and Compounds 509 (2011) 609–613

Contents lists available at ScienceDirect

Journal of Alloys and Compounds

journal homepage: www.elsevier.com/locate/jallcom

Fabrication of antimony telluride nanoparticles using a brief chemical synthetic process under atmospheric conditions

Cham Kim[a,b], Dong Hwan Kim[a], Yoon Soo Han[a], Jong Shik Chung[b], Hoyoung Kim[a,*]

[a] Daegu Gyeongbuk Institute of Science and Technology (DGIST), 711-623 Hosan-dong, Dalseo-gu, Daegu 704-230, Republic of Korea
[b] Department of Chemical Engineering, Pohang University of Science and Technology (POSTECH), San 31 Hyoja-dong, Pohang 790-784, Republic of Korea

ARTICLE INFO

Article history:
Received 22 July 2010
Received in revised form
28 September 2010
Accepted 4 October 2010
Available online 25 October 2010

Keywords:
Sb_2Te_3 nanoparticles
Thermoelectric
Chemical synthesis
L-Tartaric acid
$NaBH_4$

ABSTRACT

Antimony telluride (Sb_2Te_3) nanoparticles for thermoelectric applications were successfully prepared via a water-based chemical reaction under atmospheric conditions. In this process, we tried to prepare the nanostructured compound by employing both a complexing agent (L-tartaric acid) and a reducing agent ($NaBH_4$) to stabilize the Sb precursor ($SbCl_3$) in water and to favor the reaction with Te. It was observed that various products of Te, Sb_2O_3, and Sb_2Te_3 were individually or simultaneously generated depending on the amount of the complexing and reducing agents used. In order to obtain solely a rhombohedral Sb_2Te_3 compound, the aging time of the reaction needed to be adjusted.

1. Introduction

Thermoelectric (TE) generation has been intensively researched due to its attractive applications such as waste heat-to-electricity conversion and solid-state cooling [1–7]. In this field, one of the main topics has always been how to improve the performance of TE materials to increase the efficiency of TE devices. The comprehensive performance of such materials is evaluated via the dimensionless figure of merit $ZT(=\alpha^2\sigma T/\kappa)$, where α is the Seebeck coefficient, σ is the electrical conductivity, T is the absolute temperature, and κ is the thermal conductivity [5–10]. Therefore, an excellent TE material should have both a high σ and a low κ, which are characteristics indicative of a so-called phonon-glass/electron-crystal (PGEC) [1,7,8–15].

With meteoric development in nanotechnology, many groups have been trying to build low-dimensional structures to use as PGEC materials. Reports have shown that ZT can be enhanced in the structures of quantum dots (QD) and superlattice (SL) thin films due to both the increase in the power factor ($\alpha^2\sigma$) and the decrease in κ, which result from quantum confinement and the phonon scattering effect, respectively [13–21]. Relatively high ZT values were often exhibited in these QDs or SL structures, but it has generally been known that commercial use of these substances is difficult due to complicated production processes and high costs. Therefore, some groups are focusing on the approach using nanobulk structures such as nanoparticles [22–24], nanotubes [25–27], and nanowires [28–30]. Not only do these nanostructures still have the phonon scattering effect, which reduces κ, but they also can be prepared using cheaper processes.

In the present study, we intended to develop Sb_2Te_3 nanoparticles via a brief chemical synthetic route for the application to low-temperature operations (0–250 °C). The stabilization and the dissolution of precursors were accomplished in water using chemical additives, and the overall reaction was carried out using different aging conditions. Although we did not use a toxic organic solvent and we just conducted the aging process under ambient condition (without high pressure) unlike other works [31,32], our product was confirmed to show the single crystalline structure without any second phases and more homogeneous particle size distribution. The crystalline structures and the particle size distributions of the products were characterized, and the influences of various reaction conditions on the results were discussed. Consequently, we demonstrated that pure Sb_2Te_3 nanoparticles, which were highly dispersed and well crystallized, were successfully fabricated via a brief chemical synthetic route under ambient conditions.

2. Experimental details

2.1. Chemicals

Antimony(III) chloride ($SbCl_3$, Aldrich, ACS reagent) and Te powder (Kojundo chemical, 99.999%, 45 μm) were employed as precursors. L-Tartaric acid (TA:

* Corresponding author. Tel.: +82 54 770 2936; fax: +82 54 770 2940.
E-mail addresses: hoykim@dgist.ac.kr, kc0207@postech.ac.kr (H. Kim).

0925-8388/$ – see front matter © 2010 Elsevier B.V. All rights reserved.
doi:10.1016/j.jallcom.2010.10.002

$HO_2CCH(OH)CH(OH)CO_2H$, Aldrich, ACS reagent) and sodium borohydride ($NaBH_4$, Aldrich, ACS reagent) were used to form Sb complex ions and to reduce them with Te, respectively. All of the chemicals were used without any further purification.

2.2. Sample preparation

$SbCl_3$ was mixed with deionized (DI) water, and various amounts of the complexing agent, TA, were added. The resulting white suspension was vigorously stirred until a homogeneous solution was formed without any precipitation (solution A). Meanwhile, Te was placed in a two-neck round-bottom flask, and the flask was purged with N_2, after which the reducing agent, $NaBH_4$(aq), was added. This Te mixture was heated to 120 °C with vigorous stirring. When the mixture completely turned into a transparent purple-colored solution, solution A was added dropwise with a syringe. After the resulting black compound was refluxed for 6–12 h, it was filtered and rinsed thoroughly using dry ethanol and DI water. The product was dried under vacuum at 60 °C overnight.

2.3. Characterization

Powder X-ray diffraction (XRD) patterns were collected with a D/MAX-2500 diffractometer (Rigaku) using Cu Kα radiation and a scintillation counter detector. Relevant patterns were recorded in the 2θ range of 20–80°. Field emission scanning electron micrographs were obtained using an S-4800 FE-SEM (Hitachi) to observe the relevant morphology. The atomic composition ratios of the products were measured via inductively coupled plasma spectroscopy (ICP, Flame Modula S, Spectro).

3. Results and discussion

Unlike most of the chloride-type metal salts, $SbCl_3$ is easy to hydrolyze to form antimony(III) oxychloride, SbOCl, in an aqueous solution (Eq. (1)). Because of the extensive precipitation of SbOCl in this system, it is impossible to produce the desired nanoparticles without using a complementary treatment. Therefore, some researchers have used hydrochloric acid (HCl) to dissolve $SbCl_3$ in order to obtain stabilized Sb^{3+} ions in water. If the appropriate amount of HCl is added to the precipitate, Sb^{3+} ions can effectively be dispersed in

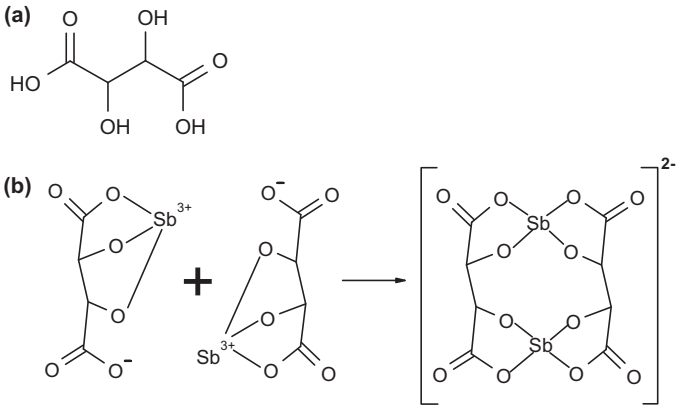

Fig. 1. Structural formula of L-tartaric acid (a) and formation mechanism of the antimony tartrate anion, $[Sb_2(C_4H_2O_6)_2]^{2-}$, which stabilizes Sb^{3+} in an aqueous solution (b).

$$SbCl_3(aq) + H_2O(l) \leftrightarrow SbOCl(s) + 2HCl(aq) \quad (1)$$

water. This treatment is based on Le Chatelier's principle; however, a strong acid could not be used in the present study since the Te source (Te powder) should easily be oxidized at a low pH, which would prevent Te from reacting with the Sb^{3+} ions in the system. Therefore, we took note of some organic acids, which are known to play a role in stabilizing metal ions, and we expected

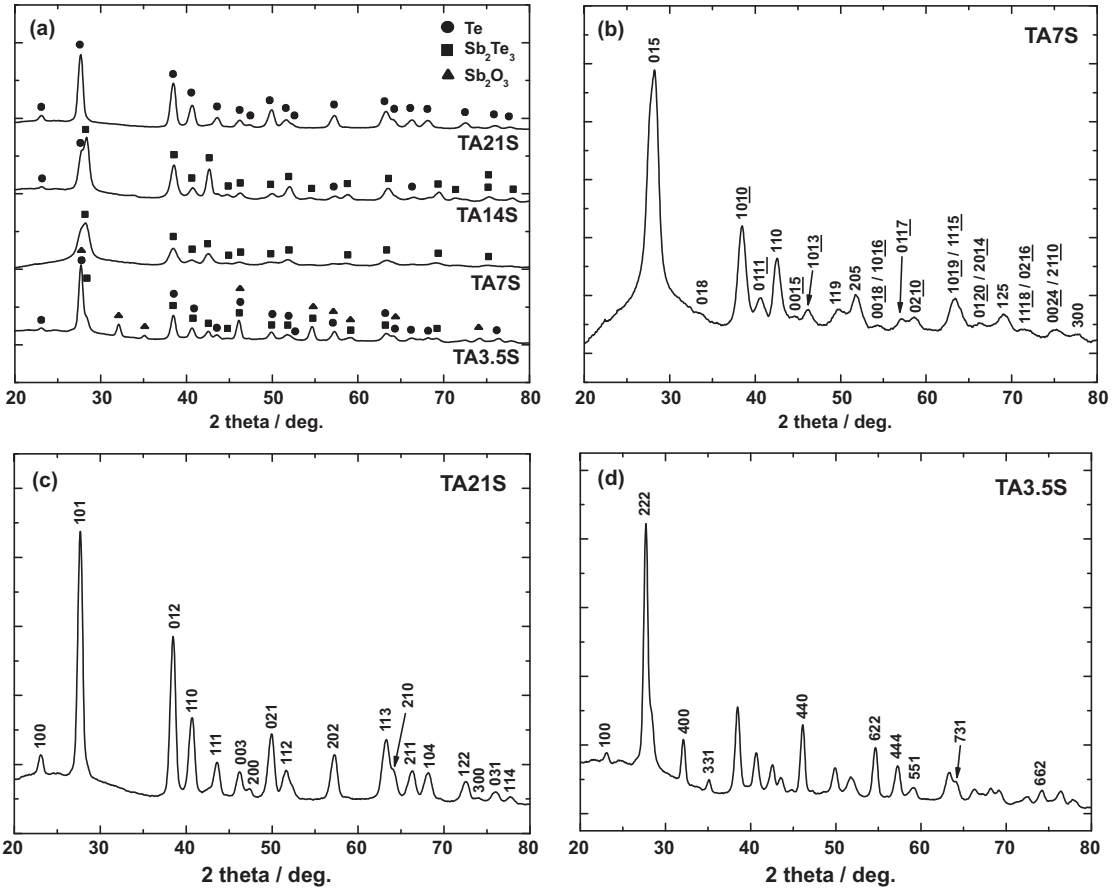

Fig. 2. Effect of the amount of L-tartaric acid on the crystalline structures of the products: comparison of the diffraction patterns of the products (a) and presentation of each crystalline direction (b–d).

them to generate complexes stabilized with organic ligands, such as Sb(III)-complexes, in water. Tella and Pokrovski arranged the stability and structure of Sb(III) with various organic compounds having O-bearing functional groups (carboxyl or hydroxyl groups) in aqueous solution [33]. They reported that some poly-functional carboxylic or hydroxyl-carboxylic acids can form Sb(III)-complexes over a wide pH range ($3 < pH < 9$), whereas the hydrolyzed species, $Sb(OH)_3$, is mainly detected with mono-functional organic compounds, indicating the poor complexing ability of mono-functional organic compounds. Accordingly, we considered adopting the poly-functional acids for the present study, and we finally chose L-tartaric acid (TA) as the complexing agent due to its numerous functional groups and its high dissociation constant. The chemical formula of TA and the formation mechanism of antimony tartrate anion are presented in Fig. 1. As shown in Fig. 1a, TA has two carboxylic groups and hydroxyl groups (poly-functional O-bearing organic ligand). An Sb^{3+} ion is possibly attracted to one carboxylic group and two hydroxyl groups of TA, resulting in a 1:1 stoichiometry for the Sb(III)-TA complex. Then, the remaining carboxylic group of TA interacts with the Sb(III) of another complex; thus the antimony tartrate anion, $[Sb_2(C_4H_2O_6)_2]^{2-}$ is formed. This mechanism was first described by Kamenar et al. in 1969 and has subsequently been described and applied by many researchers [33–35].

Although the theoretical stoichiometric ratio (TA/Sb(III)) was known to be 1 for the stabilization, the molar ratio of TA and $SbCl_3$ actually required could be different since $SbCl_3$ is largely hydrolyzed in water and large amounts of SbOCl should instantly form instead of generating free Sb^{3+}. Due to this fact, we first tried to search for the most appropriate ratio of TA to $SbCl_3$ (TA/$SbCl_3$) in the present study. TA was gradually added to a mixture of $SbCl_3$ and deionized water until a transparent solution was obtained. When the ratio was fixed at ca. 3.5, a clear solution was observed. This solution was referred to as TA3.5S, and TA–Sb(III) complexes ($[Sb_2(C_4H_2O_6)_2]^{2-}$) with different TA/$SbCl_3$ ratios were also prepared (TA7S: 7.0, TA14S: 14, TA21S: 21). We reacted each of these complexes separately with the reduced Te source (HTe^-), which had previously been prepared (Eq. (2)), and we aged these reaction mixtures for 6 h to form the desired product, Sb_2Te_3 (Eq. (3)). According to the crystalline patterns of the

$$BH_4^- + Te \rightarrow BH3 + HTe^- \quad (2)$$

$$[Sb_2(C_4H_2O_6)_2]^{2-} + 3HTe^- \rightarrow Sb_2Te_3 + 2(C_4H_2O_6)^{4-} + 3H^+ \quad (3)$$

resulting products (Fig. 2a), it was confirmed that the components in solution were largely affected by the TA/SbCl3 ratio. Most importantly, TA7S showed the single-phase rhombohedral structure of Sb_2Te_3, having the diffraction lines of (0 1 5), (0 1 8), (1 0 $\underline{10}$), (0 1 $\underline{11}$), (1 1 0), (0 0 $\underline{15}$), (1 0 $\underline{13}$), (1 1 9), (2 0 5), (0 0 $\underline{18}$/1 0 $\underline{16}$), (0 1 $\underline{17}$), (0 2 $\underline{10}$), (1 0 $\underline{19}$/1 1 $\underline{15}$), (0 1 $\underline{20}$/2 0 $\underline{14}$), (1 2 5), (1 1 $\underline{18}$/0 2 $\underline{16}$), (0 0 $\underline{24}$/2 1 $\underline{10}$), and (1 1 0) planes at 2θ values of 28.3°, 33.1°, 38.2°, 41.1°, 42.5°, 44.5°, 45.2°, 49.8°, 52.0°, 54.2°, 57.0°, 58.5°, 63.2°, 66.1°, 68.7°, 72.1°, 75.3°, and 77.5°, respectively, which exactly coincide with the values of JCPDS card No. 71–0393 (Fig. 2b).

Similarly, unwanted constituents were also detected when the samples were prepared with higher or lower TA / $SbCl_3$ ratios than that of TA7S. We found that Te began to come out of the rhombohedral phase of Sb_2Te_3 when the ratio was 14:1 (TA14S in Fig. 2a). If the ratio was increased to 21:1 (TA21S in Fig. 2a), the rhombohedral phase was completely converted into the hexagonal structure of Te (JCPDS card No. 86–2269) with the crystalline planes of (1 0 0), (1 0 1), (0 1 2), (1 1 0), (1 1 1), (0 0 3), (2 0 0), (0 2 1), (1 1 2), (2 0 2), (1 1 3), (2 1 0), (2 1 1), (1 0 4), (1 2 2), (3 0 0), (0 3 1), and (1 1 4) at 23.1°, 27.7°, 38.5°, 40.7°, 43.6°, 46.2°, 47.4°, 49.9°, 51.6°, 57.2°, 63.3°, 64.2°, 66.4°, 68.2°, 72.5°, 74.1°, 76.0°, and 77.7°, respectively (Fig. 2c). These results indicate that the reaction rate between TA–Sb(III) and HTe^- gradually diminished with an increasing amount of TA. In other words, when more TA was used in the reaction, its complexing effect was enhanced, leading to inhibition of the reactivity of Sb^{3+}. As a result, HTe^- was not able to react with Sb^{3+}, and Te therefore increasingly precipitated in the system. TA–Sb(III) complexes were expected to remain during this reaction step but could have been removed from the system via the washing step. Therefore, the end product only exhibited the hexagonal phase of Te, as shown in Fig. 2c.

In contrast, we detected three different diffraction patterns when setting the ratio at 3.5 (TA3.5S). A third crystalline structure was found in TA3.5S in addition to the rhombohedral Sb_2Te_3 and the hexagonal Te, which also appeared in TA7S and TA21S, respectively (Fig. 2a). The structure was identified as the cubic Sb_2O_3 (JCPDS card No. 5–534) having the crystalline planes of (1 0 0), (2 2 2), (4 0 0), (3 3 1), (4 4 0), (6 2 2), (4 4 4), (5 5 1), (7 3 1), and (6 6 2) at 23.1°, 27.7°, 32.1°, 35.1°, 46.1°, 54.6°, 57.2°, 59.1°, 64.1°, and 74.2°, respectively (Fig. 2d). In this case, some $SbCl_3$ might have formed TA–Sb(III) complexes, but the remnant was likely hydrolyzed to form SbOCl due to the insufficient amount of TA present. It seems that the SbOCl precipitates were further oxidized during the process, resulting in the formation of Sb_2O_3. Therefore, some HTe^- ions should have reacted with the TA–Sb(III) complexes resulting in the formation of Sb_2Te_3; however, the rest of the HTe^- ions must have re-precipitated as Te particles since they could not react with the Sb_2O_3 particles. Consequently, TA3.5S has three different crystalline phases, which are cubic Sb_2O_3, rhombohedral Sb_2Te_3, and hexagonal Te.

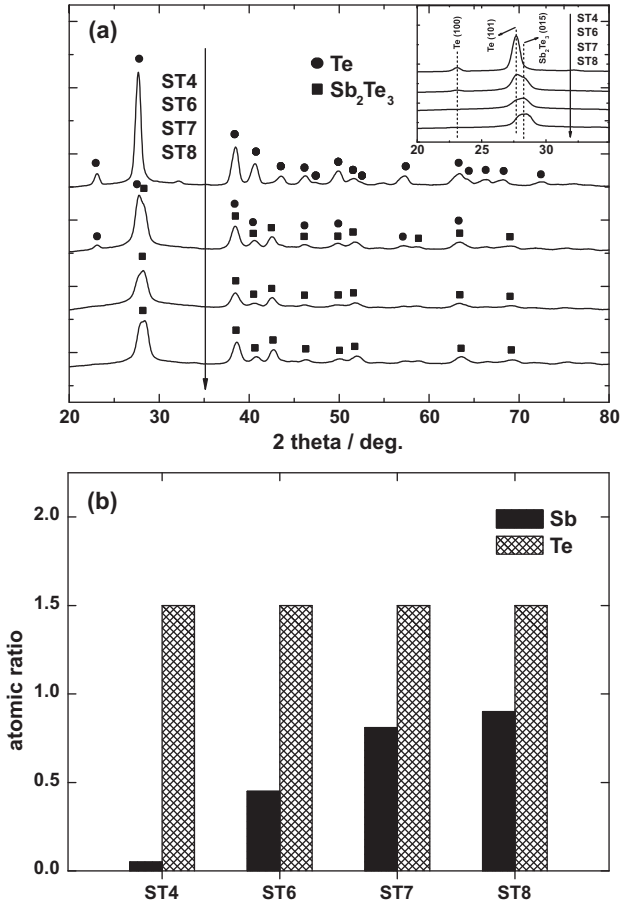

Fig. 3. Gradual conversion of the crystalline structures of the products fabricated under different concentrations of $NaBH_4$ (a) and their atomic composition ratios (b).

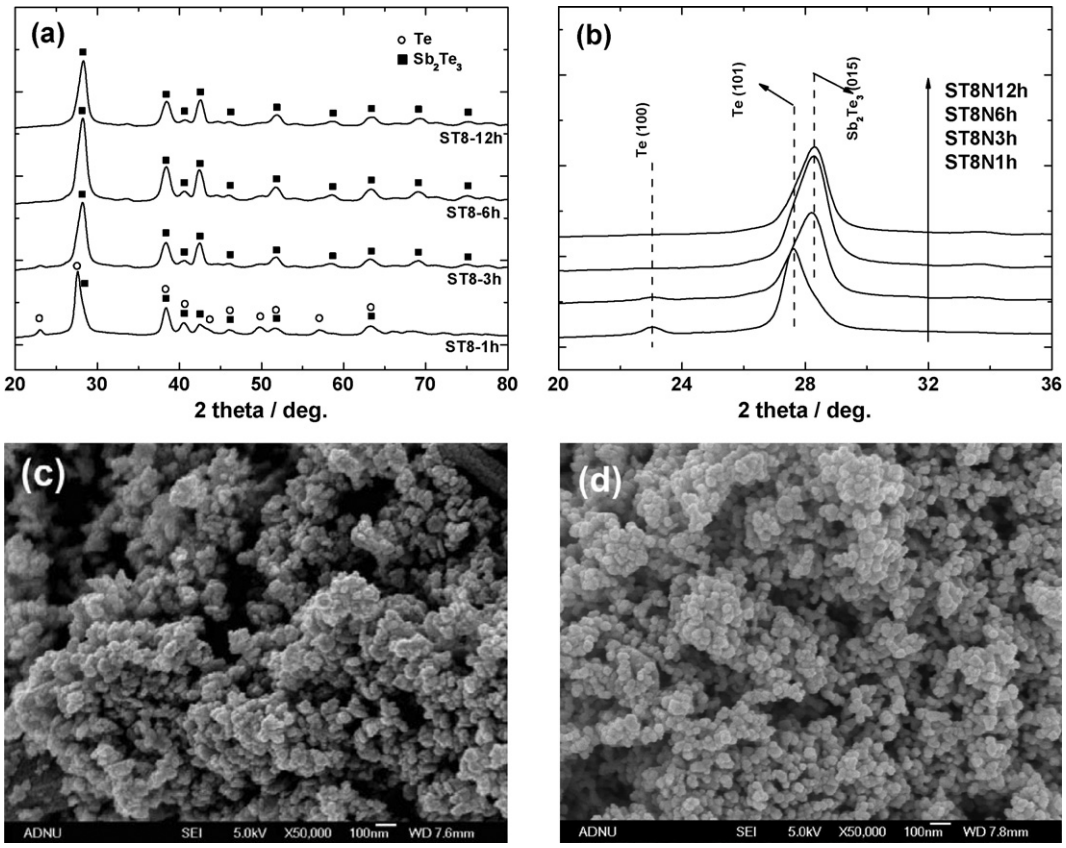

Fig. 4. Overall and enlarged diffraction patterns of the products formed using different reaction times (a and b) and the observed morphology of the products aged for 6 h (c) and 12 h (d).

Although we have optimized the TA/$SbCl_3$ ratio (TA7S: 7.0) to obtain single-phase Sb_2Te_3 nanoparticles, we still doubted whether the product was homogeneous since its phase could greatly be affected by other factors. In the present study, we also paid attention to the amount of a reductant ($NaBH_4$) used. If sufficient $NaBH_4$ is not supplied to the system, Te would not be reduced and would remain in the final product. The crystalline structures of the samples prepared with different concentrations of $NaBH_4$ are shown in Fig. 3a (ST4: 0.08 M, ST6: 0.16 M, ST7: 0.24 M, ST8: 0.32 M). It was confirmed that the crystalline structure of the sample varied considerably from hexagonal Te to rhombohedral Sb_2Te_3 as the $NaBH_4$ concentration was increased. In the case of ST4, Te would be left behind without a further reaction with the TA–Sb(III) complex because it was barely reduced due to the lack of $NaBH_4$. Thus, most of the complex was likely discharged from the system, and a single-phase hexagonal Te was obtained. These results were in good agreement with the ICP measurements – ST4 was mainly composed of Te (Fig. 3b). Meanwhile, the diffraction lines indicated that rhombohedral Sb_2Te_3 started to appear in ST6 with relatively weakened hexagonal Te, and the whole phase was finally converted into the rhombohedral Sb_2Te_3 structure in ST7. These results indicate that Te was adequately reduced to HTe^- by sufficient $NaBH_4$ in ST7 but not in ST6. In other words, when ST6 was prepared, both reduced and unreduced Te coexisted due to the insufficient amount of $NaBH_4$. Obviously, the reduced Te should react with the TA–Sb(III) complex, resulting in the formation of Sb_2Te_3, but the unreduced Te remained in the system in the form of hexagonal Te without undergoing further reaction. Therefore, some of the TA–Sb(III) complex must have been removed during washing step when ST6 was prepared. Consequently, ST7 exhibited an atomic ratio (Sb:Te = 0.84:1.5) close to that of the theoretical stoichiometry between the two atoms (1:1.5), whereas ST6 still showed the Sb-deficient ratio (0.38:1.5), as presented in Fig. 3b.

We closely examined the crystalline structure of ST7, since it was still questionable whether the sample had the single-phase rhombohedral structure of Sb_2Te_3 (Fig. 3a, inlet). The (0 1 5) plane of Sb_2Te_3 was slightly increased from ST4 to ST8, while both the (1 0 0) and (1 0 1) planes of Te were weakened. The main peak of ST7, however, became asymmetric when it was divided at the 2θ value of 28.3°, which corresponds to the (0 1 5) plane of Sb_2Te_3. This implies that the Te diffraction line of the (1 0 1) plane still existed in ST7. Therefore, we tried to prepare the sample with a higher concentration of $NaBH_4$ (ST8). The entire diffraction pattern of ST8 was almost same as that of ST7, as indicated in Fig. 3a, but its main peak was shifted slightly to a higher angle side compared to that of ST7 – the main peak was located at precisely 28.3° (Fig. 3a, inlet). As a result, the hexagonal Te completely disappeared in ST8; therefore, we obtained the desired structure: single-phase rhombohedral Sb_2Te_3. The atomic ratio of ST8 (0.92:1.5) was closer to the theoretical stoichiometry than that of ST7 but still showed a slight error (Fig. 3b). Although we further increased the $NaBH_4$ concentration, no considerable change was detected in the atomic ratio; thus, the error seemed to be caused by a lack of $SbCl_3$, which was initially supplied, or by inaccuracy of the ICP measurement.

As we already mentioned above, the reaction between TA–Sb(III) and HTe^- was run for only 6 h (aging time) from the moment when the reaction components were mixed. To verify the effect of aging time on the product composition, we varied the time from 1 to 12 h. ST8 samples were prepared with various aging times, and their crystalline patterns are shown in Fig. 4a (ST8-*X*, *X*: aging time). The reaction did not seem to be completed when the samples were aged for less than 6 h. In the case of ST8-1 h, many diffraction

lines of Te were still observed, especially the lines corresponding to the Te (1 0 0) and (1 0 1) planes (Fig. 4b). We considered that the Te-rich mixture, ST8-1 h, was generated because most TA–Sb(III) complexes could not react with HTe^- during such a short aging time and were likely removed during the washing process. In the case of ST8-3 h, both the Te planes became remarkably weakened when compared to those of ST8-1 h since the complete rate of the reaction between TA–Sb(III) and HTe^- should become higher with increased aging time. The Te phase, however, still appeared in ST8-3 h because its main peak was somewhat shifted to the direction of the Te (1 0 1) plane as shown in Fig. 4b. The reaction was considered to be complete when the samples were aged for more than 6 h since we did not find any remarkable difference between the main peaks of ST8-6 h and ST8-12 h (Fig. 4b). ST8-12 h showed the single-phase rhombohedral structure of Sb_2Te_3, which was almost the same as that of ST8-6 h, as presented in Fig. 4a. This indicates that the reaction was likely complete about 6 h after it was initiated. We also confirmed that the particle size and distribution were not largely affected by aging time if the reaction was maintained for more than 6 h – both the samples were composed of Sb_2Te_3 nanoparticles under 100 nm with similar distributions (Fig. 4c and d). Therefore, aging times between 6 and 12 h resulted in rhombohedral Sb_2Te_3 nanoparticles with good distributions.

We have shown that the final phases of products largely depended on reaction parameters such as chemical additives and the aging time. The experimental data exhibited in the present study showed the influence of each parameter on the products. We used the data to optimize the reaction conditions and finally obtained the desired product: highly dispersed single-phase Sb_2Te_3 nanoparticles. Manufacturing sintered bodies is now being investigated to measure the thermoelectric performance (ZT) of the nanoparticles and to feasibly apply them to thermoelectric modules.

4. Conclusions

In this study, we tried to prepare Sb_2Te_3 thermoelectric nanoparticles using a water-based chemical reaction under atmospheric conditions. In order to obtain only a rhombohedral Sb_2Te_3, we varied some of the reaction parameters, such as the amount of chemical agents (TA and $NaBH_4$) and the aging time. The chemical and physical properties of the products turned out to be largely affected by the parameters. Finally, we obtained the desired thermoelectric Sb_2Te_3 nanoparticles having a single crystalline structure with the appropriate atomic composition.

Acknowledgements

This work was supported by the DGIST Basic Research Program of the Ministry of Education, Science and Technology. It was also supported by the Energy Efficiency & Resources of the Korea Institute of Energy Technology Evaluation and Planning (KETEP) grant funded by the Ministry of Knowledge Economy, Republic of Korea (No. 2007EID11P050000).

References

[1] M.S. Dresselhaus, G. Chen, M.Y. Tang, R.G. Yang, H. Lee, D.Z. Wang, Z.F. Ren, J.P. Fleurial, P. Gogna, Adv. Mater. 19 (2007) 1.
[2] M.S. Dresselhaus, G. Chen, M.Y. Tang, R.G. Yang, H. Lee, D.Z. Wang, Z.F. Ren, J.P. Fleurial, P. Gogna, Mater. Res. Soc. Symp. Proc. 886 (2006), 0886-F01-01.1.
[3] D.F. Byrnes, B. Heshmatpour, Mater. Res. Soc. Symp. Proc. 886 (2006), 0886-F12-03.1.
[4] T.M. Tritt, B. Zhang, N. Gothard, J. He, X. Ji, D. Thompson, J.W. Kolis, Mater. Res. Soc. Symp. Proc. 886 (2006), 0886-F02-01.1.
[5] J. Sootsman, H. Kong, C. Uher, A. Downey, J.J. D'Angelo, C.-I. Wu, T. Hogan, T. Caillat, M. Kanatzidis, Mater. Res. Soc. Symp. Proc. 1044 (2008), 1044-U08-01.
[6] K.F. Hsu, S. Loo, F. Guo, W. Chen, J.S. Dyck, C. Uher, T. Hogan, E.K. Polychroniadis, M.G. Kanatzidis, Science 303 (2004) 818.
[7] X. Ji, B. Zhang, T.M. Tritt, J.W. Kolis, A. Kumbhar, J. Electron. Mater. 36 (2007) 721.
[8] T.J. Zhu, Y.Q. Liu, X.B. Zhao, Mater. Res. Bull. 43 (2008) 2.
[9] A. Rey, M. Faraldos, J.A. Casas, J.A. Zazo, A. Bahamonde, J.J. Rodríguez, Key Eng. Mat. 368–372 (2008) 550.
[10] J. Martin, G.S. Nolas, W. Zhang, L. Chen, Appl. Phys. Lett. 90 (2007) 222112.
[11] G.J. Snyder, M. Christensen, E. Nishibori, T. Caillat, B.B. Iversen, Nat. Mater. 3 (2004) 458.
[12] G.S. Nolas, J. Sharp, H.J. Goldsmid, Thermoelectrics: Basic Prinsicples New Materials Developments, Springer, 2001.
[13] K. Kurosaki, T. Matsuda, M. Uno, S. Kobayashi, S. Yamanaka, J. Alloys Compd. 319 (2001) 271.
[14] H.J. Goldsmid, Introduction to Thermoelectricity, Springer, 2009.
[15] J. Peng, J. He, P.N. Alboni, T.M. Tritt, J. Electron. Mater. 38 (2009) 981.
[16] G.S. Nolas, D.T. Morelli, T.M. Tritt, Annu. Rev. Mater. Sci. 29 (1999) 89.
[17] Gao Min, D.M. Rowe, J. Mater. Sci. Lett. 18 (1999) 1305.
[18] A. Grytsiv, P. Rogl, S. Berger, C. Paul, H. Michor, E. Bauer, G. Hilscher, C. Godart, P. Knoll, M. Musso, W. Lottermoser, A. Saccone, R. Ferro, T. Roisnel, H. Noel, J. Phys.: Condens. Matter. 14 (2002) 7071.
[19] J. Tang, T. Rachi, R. Kumashiro, M.A. Avila, K. Suekuni, T. Takabatake, F.Z. Guo, K. Kobayashi, K. Akai, K. Tanigaki, Phys. Rev. B 78 (2008) 085203.
[20] R.P. Hermann, F. Grandjean, V. Keppens, W. Schweika, G.S. Nolas, D.G. Mandrus, B.C. Sales, H.M. Christen, P. Bonville, Gary J. Long, Mater. Res. Soc. Symp. Proc. 886 (2005), 0886-F10-01.
[21] S. Paschen, V. Pacheco, A. Bentien, A. Sanchez, W. Carrillo-Cabrera, M. Baenitz, B.B. Iversen, Yu. Grin, F. Steglich, Phys. B 328 (2003) 39.
[22] Y. Deng, X. Zhou, G. Wei, J. Liu, C.-W. Nan, S. Zhao, J. Chem. Solids 63 (2002) 2119.
[23] X. Ji, X. Zhao, Y. Zhang, B. Lu, H. Ni, Mater. Res. Soc. Symp. Proc. 793 (2004), S1.4.1.
[24] B. Poudel, Q. Hao, Y. Ma, Y. Lan, A. Minnich, B. Yu, X. Yan, D. Wang, A. Muto, D. Vashaee, X. Chen, J. Liu, M.S. Dresselhaus, G. Chen, Z. Ren, Science 320 (2008) 634.
[25] X.B. Zhao, X.H. Ji, Y.H. Zhang, T.J. Zhu, J.P. Tu, X.B. Zhang, Appl. Phys. Lett. 86 (2005) 062111.
[26] J. Hone, I. Ellwood, M. Muno, A. Mizel, M.L. Cohen, A. Zettl, A.G. Rinzler, R.E. Smalley, Phys. Rev. Lett. 80 (1998) 1042.
[27] Y.Q. Cao, T.J. Zhu, X.B. Zhao, J. Alloys Compd. 449 (2008) 109.
[28] J. Lu, Q. Han, X. Yang, L. Lu, X. Wang, Mater. Lett. 61 (2007) 3425.
[29] X.B. Zhao, X.H. Ji, Y.H. Zhang, B.H. Lu, J. Alloys Compd. 368 (2004) 349.
[30] T. Sun, X.B. Zhao, T.J. Zhu, J.P. Tu, Mater. Lett. 60 (2006) 2534.
[31] Kyung Tae Kim, Dong-Won Kim, Gil-Geun Lee, Gook Hyun Ha, Adv. Power Technol. (2010), in press, doi:10.1016/j.apt.2010.08.006.
[32] W. Ren, C. Cheng, Y. Xu, Z. Ren, Y. Zhong, J. Alloys Compd. 501 (2010) 120.
[33] Marie Tella, Gleb S. Pokrovski, Geochim. Cosmochim. Acta 73 (2009) 268.
[34] I.O. Mazali, W.C. Las, M. Cilense, J. Mater. Synth. Proces. 7 (1999) 387.
[35] S.R. Gadakh, C.H. Bhosale, Mater. Chem. Phys. 78 (2002) 367.